A global perspective on Langmuir turbulence in the ocean surface boundary layer

Stephen E. Belcher,[1,2] Alan L. M. Grant,[1] Kirsty E. Hanley,[1] Baylor Fox-Kemper,[3,4] Luke Van Roekel,[4,5] Peter P. Sullivan,[6] William G. Large,[6] Andy Brown,[2] Adrian Hines,[2] Daley Calvert,[2] Anna Rutgersson,[7] Heidi Pettersson,[8] Jean-Raymond Bidlot,[9] Peter A. E. M. Janssen,[9] and Jeff A. Polton[10]

Received 29 June 2012; revised 13 August 2012; accepted 14 August 2012; published 21 September 2012.

[1] The turbulent mixing in thin ocean surface boundary layers (OSBL), which occupy the upper 100 m or so of the ocean, control the exchange of heat and trace gases between the atmosphere and ocean. Here we show that current parameterizations of this turbulent mixing lead to systematic and substantial errors in the depth of the OSBL in global climate models, which then leads to biases in sea surface temperature. One reason, we argue, is that current parameterizations are missing key surface-wave processes that force Langmuir turbulence that deepens the OSBL more rapidly than steady wind forcing. Scaling arguments are presented to identify two dimensionless parameters that measure the importance of wave forcing against wind forcing, and against buoyancy forcing. A global perspective on the occurrence of wave-forced turbulence is developed using re-analysis data to compute these parameters globally. The diagnostic study developed here suggests that turbulent energy available for mixing the OSBL is under-estimated without forcing by surface waves. Wave-forcing and hence Langmuir turbulence could be important over wide areas of the ocean and in all seasons in the Southern Ocean. We conclude that surface-wave-forced Langmuir turbulence is an important process in the OSBL that requires parameterization. **Citation:** Belcher, S. E., et al. (2012), A global perspective on Langmuir turbulence in the ocean surface boundary layer, *Geophys. Res. Lett.*, *39*, L18605, doi:10.1029/2012GL052932.

1. Introduction

[2] The turbulent motions in thin ocean surface boundary layers (OSBL), which occupy the upper 100 m or so of the ocean, control the exchange of momentum, heat and trace gases between the atmosphere and ocean. The ability of the oceans to buffer atmospheric climate change by absorbing and then storing heat and radiatively important trace gases relies heavily upon the exchanges in the OSBL. More permanent storage, via subduction into the ocean interior, is also influenced by the OSBL, as it sets the boundary conditions determining deep-ocean stratification and dynamics. The OSBL is therefore critical in determining the role of global ocean circulation on climate.

[3] Figure 1 shows global maps of the depth of the mixed layer of the OSBL (discussed in Figure 2 below and diagnosed here using the density criterion described in *de Boyer Montégut et al.* [2004]) averaged seasonally from a 20-year simulation from a development version of the HadGEM3 climate model. The atmospheric model has N216 resolution and the ORCA025 ocean model has 1/4° horizontal resolution, see *Hewitt et al.* [2010]. Also shown are the percentage errors relative to the Argo float data reported in *de Boyer Montégut et al.* [2004] updated to include data up to 2008. At some locations the errors can be 100% of the observed depth. *de Boyer Montégut et al.* [2004] demonstrate robustness of their estimates to other definitions of the mixed layer depth, and the errors for example in the Southern Ocean shown in Figure 1 are larger than the differences between this climatology and *Monterey and Levitus* [1997]. Similar results are found with coarser resolution models (N96 and ORCA1, NCAR CCSM4, GFDL CM2M and CM2G at 1° resolution [see *Fox-Kemper et al.*, 2011]). In the Northern Hemisphere the errors in mixed layer depth are of both signs. But in the Southern Ocean the mixed layer is generally too shallow compared to the observations, particularly during the Southern Hemisphere summer. There are corresponding errors in sea surface temperature (Figures 1e and 1f) of 3–4°C in the Southern Ocean. *Weijer et al.* [2012] compare measurements of the Southern Ocean with calculations from the CCSM4 model. They also show that the mixed layer depth is too shallow in the Southern Ocean, particularly in the Indian and east Pacific regions where the errors are comparable to the errors shown in Figure 1. These errors lead to errors within the ocean interior in dynamically important quantities such as potential vorticity, temperature and salinity, and in transport of passive tracers such as CFC-11, because they are not subducted along the correct isopycnals. Finally, a recent parameterization of the restratification of the OSBL by submesoscale eddies [*Fox-Kemper et al.*, 2008] reduces many of the deep biases in climate models [*Fox-Kemper et al.*, 2011], but it exacerbates the shallow biases, such as in the Southern Ocean.

[1]Department of Meteorology, University of Reading, Reading, UK.
[2]Met Office Hadley Centre, Exeter, UK.
[3]Department of Atmospheric and Oceanic Sciences, University of Colorado at Boulder, Boulder, Colorado, USA.
[4]Cooperative Institute for Research in Environmental Sciences, University of Colorado at Boulder, Boulder, Colorado, USA.
[5]Atmospheric Science, Northland College, Ashland, Wisconsin, USA.
[6]National Center for Atmospheric Research, Boulder, Colorado, USA.
[7]Department of Earth Sciences, University of Uppsala, Uppsala, Sweden.
[8]Marine Research, Finnish Meteorological Institute, Helsinki, Finland.
[9]European Centre for Medium-Range Weather Forecasts, Reading, UK.
[10]National Oceanography Centre, Liverpool, UK.

Corresponding author: S. E. Belcher, Department of Meteorology, University of Reading, PO Box 243, Reading RG6 6BB, UK. (s.e.belcher@reading.ac.uk)

0094-8276/12/2012GL052932

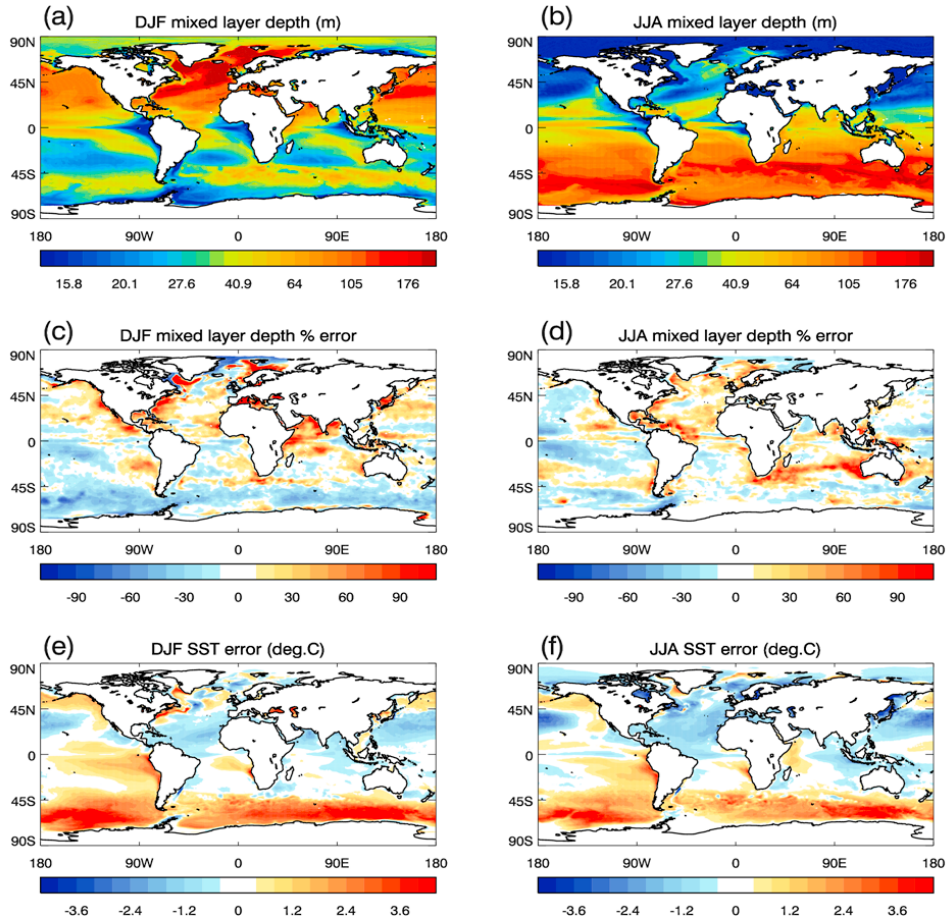

Figure 1. Seasonal variation in the OSBL depth computed with HadGEM3 averaged over 20 years and comparisons with Argo float measurements reported in *de Boyer Montégut et al.* [2004] updated to include data up to 2008: (a) computed depth DJF, (b) computed depth JJA, (c) percentage error between simulated and measured depths for DJF, (d) percentage error between simulated and measured depths for JJA. Corresponding errors in sea surface temperature: (e) DJF, (f) JJA.

[4] These results illustrate how state-of-the-art climate models produce systematic errors in the properties of the OSBL when compared to observations. In the Southern Ocean the mixed layer depth is too shallow, particularly during the Southern Hemisphere summer. Whilst atmospheric errors, for example in cloud cover and hence radiative forcing of the OSBL, could play a role, here we argue that these systematic biases have important contributions from physical, surface-wave driven, processes that are missing from current parameterizations of the OSBL. These mixed layer biases contribute (alongside atmospheric errors) to sea surface temperature errors, with many current climate models showing warm biases of several degrees in the Southern Ocean.

2. Turbulent Mixing in the Ocean Surface Boundary Layer

[5] The evolution of the OSBL is driven by a range of processes that deepen or shoal the layer [e.g., *Large et al.*, 1994; *Sullivan and McWilliams*, 2010]. Since we are concerned here with the shallow bias in climate simulations of the OSBL, we focus on processes deepening the OSBL. Figure 2 shows schematically the vertical structure of the OSBL and the processes that deepen it. The bulk of the OSBL can be termed the *mixed layer*, where the temperature and salinity are approximately uniform with depth, and which is often capped below, at the mixed layer depth, by a sharp pycnocline, which extends deeper into the ocean. Three sources of turbulence, namely wind, buoyancy and waves, drive turbulence in this mixed layer, which then deepens the OSBL. Hence a quantitative understanding of these turbulent processes in the OSBL is likely to be the key to understanding the shallow biases in mixed layer depth shown in Figure 1.

[6] Deepening of the OSBL implies an increase in potential energy, and hence requires an energy source, such as turbulent kinetic energy (hereafter TKE). The TKE equation in horizontally homogeneous flow is

$$\frac{De}{Dt} = \underbrace{-\overline{\mathbf{u}_h' w'} \cdot \frac{\partial \mathbf{u}_h}{\partial z}}_{1} \underbrace{- \overline{\mathbf{u}_h' w'} \cdot \frac{\partial \mathbf{u}_s}{\partial z}}_{2} + \underbrace{\overline{w' b'}}_{3} \underbrace{- \frac{\partial}{\partial z}\left\{ \overline{w' u_i' u_i'} + \frac{1}{\rho_0} \overline{w' p'} \right\}}_{4} - \underbrace{\varepsilon}_{5} \quad (1)$$

Here $\mathbf{u}_h$ and w are the horizontal and vertical Eulerian velocities (primes denoting turbulent fluctuations and

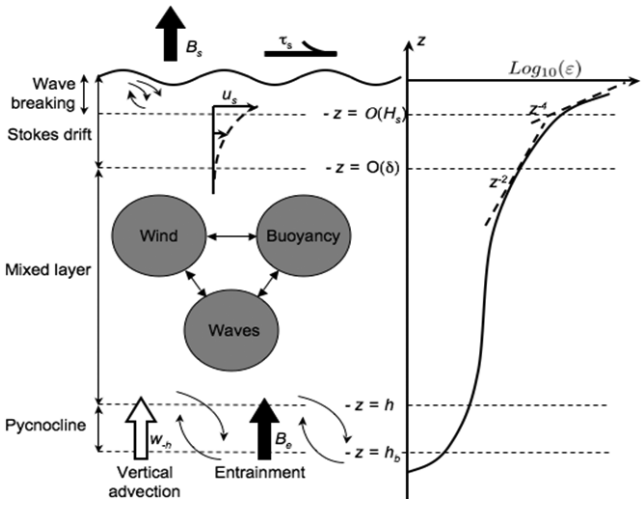

Figure 2. (left) Schematic diagram of processes deepening the OSBL and (right) vertical profile of turbulent dissipation rate, ε. The OSBL is forced at the surface by wind stress, τ_s, buoyancy flux, B_s, and surface waves through their breaking and their Stokes drift, u_s. Surface wave breaking generates turbulence, and leads to high levels of dissipation, within a distance of the order of a significant wave height, $O(H_s)$, from the surface, but does not seem to be a controlling process at deeper levels [*Terray et al.*, 1996; *Sullivan et al.*, 2007]. Stokes drift associated with the non-breaking waves penetrates a deeper distance of order $\delta = 1/2k$ (k is the wave number of waves at the peak in the wave spectrum). Stokes drift deforms absolute vorticity into the horizontal generating streamwise vortices of Langmuir turbulence [*Craik and Leibovich*, 1976; *Teixeira and Belcher*, 2002]. Below is a mixed layer where the character of the turbulence is controlled by the strength of the surface wind, buoyancy and waves (via Stokes drift) [*Grant and Belcher*, 2009]. At the base of the mixed layer, at depth h, is a pycnocline to the base of the OSBL at depth h_b, which deepens through a combination of vertical advection and entrainment by mixed-layer turbulence of denser fluid from below into the OSBL, leading to a buoyancy flux B_e.

overbar time mean), $\mathbf{u}_s$ is the Stokes drift vector associated with the surface waves, e is the turbulent kinetic energy, b' is the turbulent buoyancy fluctuation, p' turbulent pressure fluctuation and ρ background density.

[7] As indicated in Figure 2, within the mixed layer of the OSBL three processes produce TKE on the right hand side of equation (1). Term 1 is *wind-forced production*, which arises from work done on the gradient of the local Eulerian mean current generated by wind forcing at the ocean surface. (When the OSBL is shallow there can also be strong additional shear production at the base of the layer [*Large and Crawford*, 1995; *Grant and Belcher*, 2011] but this case is not considered here.) Term 2 is *wave-forced production*, which arises from work done on the gradient of the Stokes drift associated with ocean surface waves. This term gives rise to Langmuir turbulence, a fully turbulent flow with elongated vortices aligned between the direction of the wind and waves [*Skyllingstad and Denbo*, 1995; *McWilliams et al.*, 1997]. Term 3 is *buoyancy-forced production*, which generates convective turbulence when there is cooling at the ocean surface. (When there is warming at the ocean surface, this process re-stratifies the OSBL and inhibits turbulent mixing, a case not considered here but estimated in *Boccaletti et al.* [2007] and *Thomas and Ferrari* [2008].) Term 4 is transport of turbulence-by-turbulence, and redistributes TKE from its level of production through the depth of the OSBL. Term 5 is the molecular dissipation of turbulence into heat.

[8] Superficially, the wind- and wave-forced production terms in equation (1) look similar. However, wave forcing preferentially drives production of vertical turbulent velocity [*McWilliams et al.*, 1997; *Teixeira and Belcher*, 2010], in the form of downwelling jets (manifest as part of the Langmuir turbulence through the redistribution term in equation (1)) that penetrate deeper than the layer directly affected by Stokes drift; they reach the base of the OSBL and generate greater entrainment than wind-driven turbulence [see *Polton and Belcher*, 2007, Figure 7]. Hence it is likely that Langmuir turbulence will be important in deepening the OSBL.

[9] Each of these three production mechanisms produces a distinct type of turbulence, with its own scaling laws. It is then natural to define a regime diagram for mixing in the OSBL based on the relative strengths of the terms producing TKE. Since there are three production terms, there are two independent ratios that define their relative magnitudes, and hence axes of the regime diagram. Here we focus on measuring the role of wave production compared to the wind and buoyant production in order to assess the likely role of Langmuir turbulence in the OSBL.

[10] The first ratio measures wind-forced production against wave-forced production, namely

$$\frac{-\overline{\mathbf{u}_h' w'} \cdot \partial \mathbf{u}_h/\partial z}{-\overline{\mathbf{u}_h' w'} \cdot \partial \mathbf{u}_s/\partial z} \sim \frac{u_*^2 u_*/h}{u_*^2 u_s/h} = \frac{u_*^3/h}{w_{*L}^3/h} = La^2. \qquad (2)$$

Here the scaling velocity and length scales for wind-forced turbulence are u_*, the friction velocity in the water and h, the depth of the mixed layer of the OSBL (see Figure 2). *Grant and Belcher* [2009] show using LES and *Harcourt and D'Asaro* [2008] argue from measurements that the scaling velocity and length scales for wave-forced turbulence are $w_{*L} = \left(u_*^2 u_s\right)^{\frac{1}{3}}$ and h. Although the Stokes drift penetrates only a distance $O(\delta = 1/2k)$, where k is the wavenumber of the peak waves, the turbulent transport (term 4 in equation (1)) distributes the wave-forced turbulence through the whole depth, h, of the layer. The velocity scale can be obtained by balancing scaling estimates of wave-forced production (term 2 in equation (1)) with dissipation (term 5 in equation (1)) [see *Grant and Belcher*, 2009]. The square of the turbulent Langmuir number, $La^2 = (u_*/u_s)$, scales the ratio of these two production terms.

[11] When the wind and waves are not aligned, *Van Roekel et al.* [2012] use LES to show that Langmuir cells form aligned between the wind and waves. They suggest a revised formula for the Langmuir number, but do not demonstrate that it collapses terms in the TKE budget. Hence we use the definition given in equation (2), with u_s, the Stokes drift, projected into the wind direction, and acknowledge their argument that including the angle effect will tend to broaden somewhat the range of the Langmuir number.

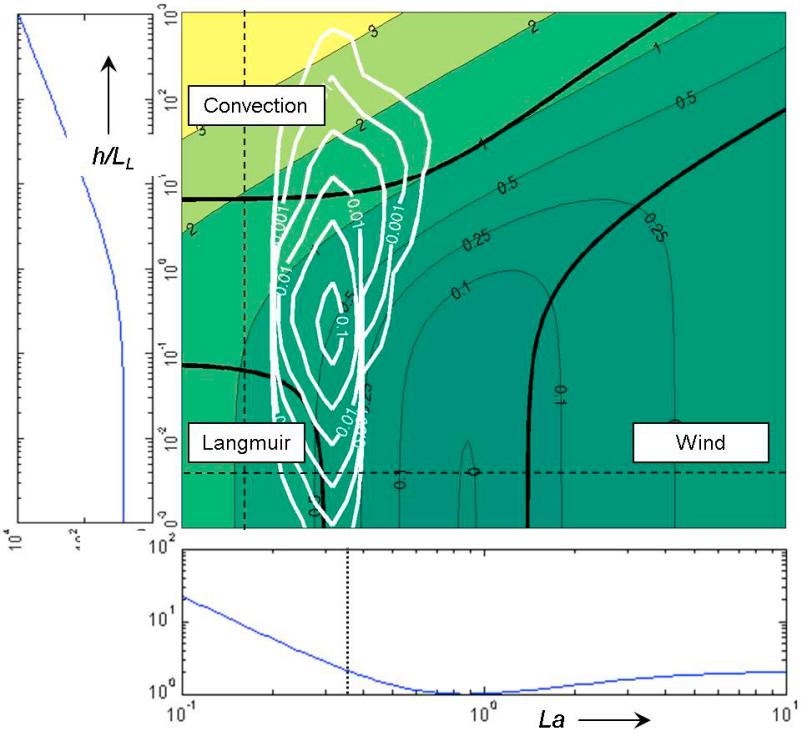

Figure 3. Regime diagram for mixing in the OSBL. Main panel: Colored contours show turbulent dissipation rate, $\log_{10}(\varepsilon h/u_*^3)$. Thick solid lines divide the regime diagram into regions where single forcings produce greater that 90% of total dissipation. Overlaid as white contours is the joint pdf of La and h/L_l computed for the Southern Ocean winter (JJA). Lower panel: Variation of $\varepsilon h/u_*^3$ with La along horizontal dashed line in main panel. The dotted line on the lower panel indicates $La = 0.35$, the value used in Figure 4. Left panel: Variation of $\varepsilon h/u_*^3$ with h/L_L along vertical dashed line in main panel.

[12] The second ratio, which has not been recognized previously, measures buoyancy-forced production against wave-forced production, and is given by

$$\frac{\overline{w'b_s'}}{-\overline{\mathbf{u}_h'w'}\cdot\partial\mathbf{u}_s/\partial z}\sim\frac{B_s}{u_*^2u_s/h}=\frac{w_*^3/h}{w_{*L}^3/h}=\frac{h}{L_L}. \tag{3}$$

Here B_s is the surface buoyancy flux (defined to be positive for an upward flux cooling the ocean). The scaling velocity and length scales for buoyancy-forced turbulence, which arise from scaling arguments for pure convection, are $w_* = (B_s h)^{\frac{1}{3}}$ and h [e.g., *Large et al.*, 1994]. The ratio in equation (3) can be written in terms of the *Langmuir stability length* $L_L = -w_{*L}^3/B_s$, which is the analogue for convective-Langmuir turbulence of the Obukhov length for convective-shear turbulence: In analogy with the convective case [*Thorpe*, 2005, p. 121], when $h/L_L < 1$ wave forcing dominates the OSBL; when $h/L_L > 1$ buoyancy forcing dominates the OSBL.

[13] A regime diagram for the OSBL can then be defined with axes $La = \left(u_*/u_s\right)^{\frac{1}{2}}$ and $h/L_L = w_*^3/w_{*L}^3$. This regime diagram is similar to the one defined by *Li et al.* [2005], but with two important differences. Firstly, here we interpret the axes as the ratio of terms that produce TKE, processes that underpin any parameterization of the OSBL mixing, whereas *Li et al.* [2005] determine their parameters from the mean momentum equation and are perhaps therefore more suitable for linear stability analysis. Secondly, Li et al.'s stability parameter is the Hoenikker number, $Ho = (4\delta/h)h/L_L$, which uses δ, the depth scale of penetration of the Stokes drift, as its length scale. Here we use the turbulent length scale, which, as argued above using term 4 of equation (1), is the mixed layer depth, h. Figure 3 shows such a regime diagram.

[14] Now, we can write turbulence quantities in terms of the scaling length and velocity scales and a dimensionless function. For example, in the mixed layer, which lies below the region near the surface directly affected by wave breaking, the dissipation rate, which is interesting because it can be measured [e.g., *D'Asaro et al.*, 2011], becomes

$$\varepsilon = \frac{U^3}{h} f_\varepsilon\left(\frac{z}{h}, La, \frac{h}{L_L}\right), \tag{4}$$

where the scaling velocity $U = u_*$, w_{*L}, or w_* for wind, wave, or buoyancy forced turbulence and $f_\varepsilon(z/h,\ La,\ h/L_L)$ is a universal function. Following the approach taken in the atmospheric boundary layer [e.g., *Moeng and Sullivan*, 1994] the dissipation in the middle of the mixed layer, for example, can be written as a linear combination of the dissipation from each the three production mechanisms, namely

$$\varepsilon(z/h = 0.5) = A_s\frac{u_*^3}{h} + A_L\frac{w_{*L}^3}{h} + A_c\frac{w_*^3}{h}, \tag{5}$$

[15] The LES results of *Grant and Belcher* [2009] are consistent with $A_s = 2\left(1 - e^{-\frac{1}{2}La}\right)$, $A_L = 0.22$. Simulations of the convective boundary layer suggest that $A_c = 0.3$ [*Moeng and Sullivan*, 1994]. This scaling applies under

uniform steady conditions: when the conditions evolve rapidly in time and space additional processes come into play, as discussed in section 4 below. The form of A_s suggests that wave-wind interaction reduces the effectiveness of shear production at moderate La, perhaps because the wave forcing generates vertical mixing that inhibits vertical current shear and thence shear-generated production. Equation (5) can be rewritten

$$\frac{\varepsilon(z/h=0.5)}{u_*^3/h} = A_s + A_L La^{-2} + A_c La^{-2}\frac{h}{L_L}. \qquad (6)$$

Figure 3 shows contours of $\log_{10}\left(\frac{\varepsilon}{u_*^3/h}\right)$ from equation (6) plotted in the $La - h/L_L$ regime diagram. The thick solid lines on this figure delineate regions where one forcing dominates at the 90% level: for example, the lower left line indicates where wave-forced production accounts for 90% of the total, suggesting that Langmuir turbulence dominates when $La < 0.3$ and $h/L_L < 0.1$. Also shown are the variation in the normalized dissipation rate with La and h/L_L.

3. A Global View of Mixing Regimes in the Ocean Surface Boundary Layer

[16] We now develop a global perspective by diagnosing the distribution of the parameters defined in section 2 using re-analysis data. We consider separately the Langmuir number and Langmuir stability parameter. The wind, wave and buoyancy forcing data are obtained from both ERA-40 [*Uppala et al.*, 2005] and ERA-Interim [*Dee et al.*, 2011], which include analyses of the two-dimensional frequency spectrum, $F(f, \phi)$ (where f is wave frequency and ϕ is wave direction), produced using a development of the WAM model, and incorporates a huge range of observations, including scatterometer measurements. The wave spectrum in ERA is computed explicitly up to $f \approx 0.41$ Hz, Higher frequencies are represented by patching on a f^{-5} tail. Following *Kenyon* [1969], the component of Stokes drift at the surface along the wind direction θ_w is computed from

$$u_s = \frac{16\pi^3}{g}\int_0^{2\pi}\int_0^{\infty} f^3 F(f,\phi)\cos(\phi-\theta_w)df\,d\phi, \qquad (7)$$

with a similar expression with $\sin(\phi - \theta_w)$ for the component perpendicular to the wind. Finally, following *Leibovich* [1983], the Langmuir number is calculated only where the 10 m-wind speed exceeds 3 m s^{-1}, which excludes about 10% of the ocean at any one time. Equation (7) then yields the component of the Stokes drift that is used in equation (2) to evaluate the Langmuir number.

3.1. A Global View of the Wind Versus Wave Forcing

[17] Figure 4 shows the global distribution of the Langmuir number. Figures 4a–4c show histograms of La for the Northern Hemisphere, the Tropics and the Southern Hemisphere, each computed using ERA-Interim and ERA-40. ERA-Interim tends to have waves more fully developed with the local wind than ERA-40, because the surface winds are stronger and because of changes to the wave model that result in wind waves developing more quickly in the presence of swell [*Dee et al.*, 2011]. The stronger Stokes drift in ERA-Interim is also in better agreement with other estimates from altimetry and different wave models [*Webb and Fox-Kemper*, 2011]. Although the analyzed wave fields are expected to be better in ERA-Interim than in ERA-40, differences in the results give some indication of our uncertainty in global estimates of La.

[18] The distributions calculated using ERA-Interim are peaked around $La = 0.3$. This value is obtained if the Stokes drift is computed from the *Pierson and Moskowitz* [1964] spectrum for waves in equilibrium with the wind, so-called fully developed seas. A value of $La = 0.3$ implies an important role for wave forcing of turbulence. The tail at higher values of La indicates conditions with more wind forcing, while the tail at lower values indicates conditions with more wave forcing, e.g., via swell from remote sources. The distributions calculated using ERA-40 peak around $La = 0.35$ and are slightly broader. The tails are consistent with *Hanley et al.* [2010], who show that in ERA-40 winds in mid-latitudes vary rapidly within synoptic systems and the waves do not reach full development. The distributions from both ERA-Interim and ERA-40 are particularly sharply peaked for the Southern Ocean, whereas in the Tropics the ERA-40 histograms are broader, with greater occurrence of higher La. This suggests a greater prevalence of Langmuir turbulence in the Southern Ocean.

[19] The f^{-5} tail contributes about 30% to the surface Stokes drift in equation (7). But this contribution originates from waves with wavelengths less that about 10 m, whose contribution to the Stokes drift penetrates only about 1 m into the water column. In this shallow region wave breaking is important, and so it is not clear whether or not they do force Langmuir turbulence. If the tail is ignored completely then the peak in the ERA-Interim distributions in Figure 4 are shifted to $La = 0.4$, implying a greater role for wind forcing. It is currently unclear which value of Stokes drift is more appropriate for the ocean, but these results demonstrate a robustness of the general conclusion of the importance of wave forcing.

[20] Conditions in enclosed seas are different compared to the open ocean. Figure 4d shows the frequency of occurrence of La using two years of turbulence and wave measurements from the Östergarnsholm site in the Baltic Sea (for a site description see *Smedman et al.* [1999] and *Rutgersson et al.* [2008]). The distribution peaks at $La = 0.35$ but is much broader than in the open ocean. In particular the distribution extends below $La < 0.3$ indicating strong wave forcing, suggesting swell dominated conditions.

[21] Figures 4e–4h show maps for winter and summer seasons computed from ERA-Interim of the frequency of occurrence of $La < 0.35$, indicating an important role for wave forcing, and $La > 0.35$, indicating a role for wind forcing. In the Southern Ocean $La < 0.35$ for more than 80% of the time throughout the year. In the North Atlantic and Pacific storm tracks La shows a stronger seasonal cycle. During the Northern Hemisphere winter La is less than 0.35 about 70% of the time. For the remainder of the time the typical range is $0.35 < La < 0.5$, indicating a role for wind forcing. During Northern Hemisphere summer, when the storm tracks are less active, $La < 0.35$ about 60% of the time, and $La > 0.35$ about 40%. In the Indian Ocean there is a strong seasonal signal associated with the monsoon. During JJA, when the monsoon is active, wave forcing is important with $La < 0.35$, whereas in DJF, when the monsoon is not

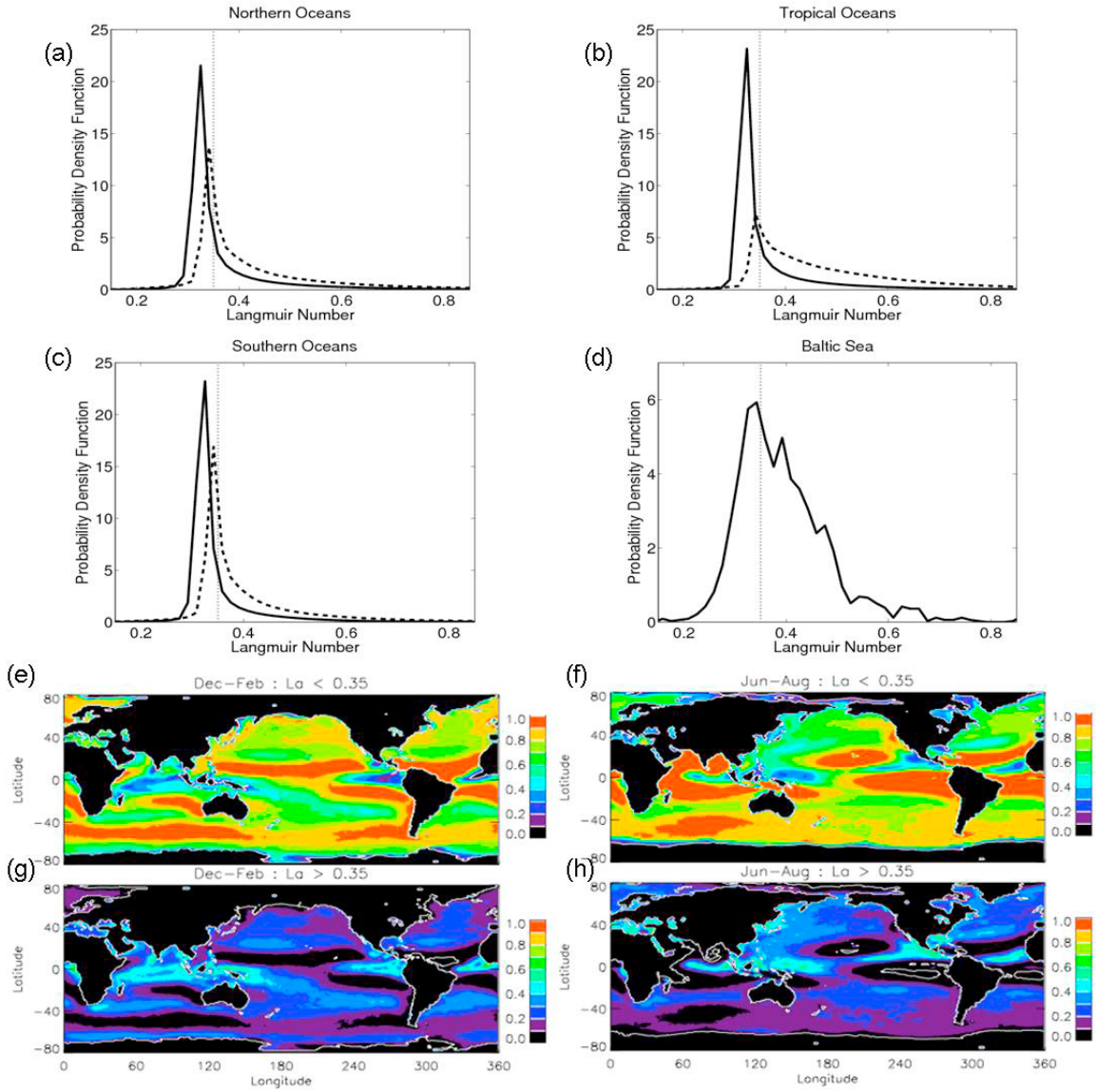

Figure 4. Global distribution of Langmuir number, *La.* istograms of *La* averaged over (a) the Northern Hemisphere, (b) the Tropics, (c) the Southern Hemisphere. Solid lines: calculated from ERA-Interim data averaged over 2000–2010; Dotted lines: ERA-40 averaged over 1992–2001. (d) Measurements from Östergarnsholm, Baltic Sea. Panels (e–h) Maps of the frequency of occurrence of $La < 0.35$ (Figures 4e and 4f) and $0.35 < La$ (Figures 4g and 4h) during December, January, February (DJF) (Figures 4e and 4g) and June, July, August (JJA) (Figures 4f and 4h), all computed from ERA-Interim.

active, *La* is distributed more evenly between wave and wind forcing. Elsewhere in the tropics $La < 0.35$.

[22] In conclusion, our synthesis of LES TKE scalings and re-analysis data indicate wave forcing of turbulence is important throughout the world's oceans. This conclusion is robust to the re-analysis used for diagnosis and to the treatment of the tail in the wave spectrum.

3.2. Buoyancy Versus Wave Forcing in the Southern Ocean

[23] The Langmuir-buoyancy stability parameter is more difficult to evaluate because, even with Argo floats, measurements of the mixed layer depth are currently available with only monthly resolution, much lower temporal resolution than the ERA-Interim data. Also, the stability length, L_L, ranges from small to very large values, so simple averages are not robust. Consequently, here a comparison of the mixed layer depths with the Langmuir-buoyancy stability lengths is preferred over computing their ratios. We focus on diagnosing the relative roles of wave and buoyancy forcing in the Southern Ocean, because of the biases identified in current models in Section 1, and because it illustrates important aspects of the competition between wave and buoyancy forcing.

[24] The Langmuir stability length, L_L, was calculated using the buoyancy flux computed from daily-averaged surface sensible and latent heat fluxes, net longwave cooling and freshwater flux from ERA-Interim. The stability length scale was calculated only when the total surface buoyancy flux was positive, i.e., cooling the ocean, when buoyancy forcing promotes convective mixing. This selection gives an upper bound on the role of buoyancy forcing in generating

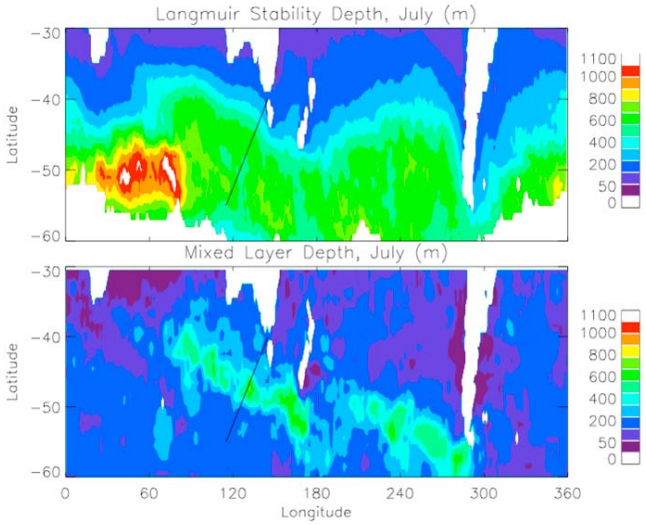

Figure 5. Roles of convectively-forced and wave-forced turbulence in the Southern Ocean during July. (top) Langmuir stability length, L_L, computed from ERA-Interim 2000–2010. (bottom) Mixed layer depth from *Dong et al.* [2008]. Notice the sharp gradient in L_L at around 40°S and the deep mixed layers south of this region. When $h > L_L$ convective forcing dominates, whereas when $h < L_L$ wave forcing dominates. A times series of these quantities along the line A-B is shown in Figure 6.

turbulence, because solar heating suppresses turbulence but with an unknown scaling. The modal average stability length over each month was then calculated.

[25] Figure 5 shows contour plots of the Langmuir stability length and measured mixed layer depth in the Southern Ocean for July, Southern Hemisphere winter. This is an interesting season because there is a band where the mixed layer is 500 m deep; elsewhere the mixed layer is between 100–200 m deep. As shown by *Dong et al.* [2008] the band of deep mixed layer lies to the south-east of the sub-Antarctic front. Climate models typically under-estimate the mixed layer depth in this region by 150 m or more (Figure 1). The Langmuir stability length increases towards the pole, mainly because the average heat flux reduces. Outside the band of deep mixed layer, h is less than L_L indicating greater importance of wave forcing over buoyancy forcing of turbulence. Within the band of deep mixed layer $h \sim L_L$, indicating wave and buoyancy forcing are comparable.

[26] Figure 6 shows a Hovmoller diagram of the mixed layer depth along the line A-B in Figure 5. This line crosses the sub-Antarctic front at about 145°E. A deep mixed layer develops to the south-east of the front during Southern Hemisphere winter, from August to October, extending eastwards to 170°E. Figure 6 (bottom) shows that the mixed layer depths reach 500 m in August and September. In this region the mixed layer depth is equal to the Langmuir-stability length, $h \sim L_L$, indicating that wave and buoyancy forcing are important. Outside this region the mixed layer depth is generally shallower than the stability length, $h < L_L$, indicating that wave forcing dominates over buoyancy forcing.

[27] This finding that wave forcing is always important when compared to buoyancy forcing even in winter is perhaps surprising: it is often thought that buoyancy forcing is the dominant process deepening the winter mixed layer. The reason can be traced to the surface buoyancy flux, which is proportional to the 10 m wind speed, the humidity contrast and the air-sea temperature difference. Over much of the ocean the humidity is high and the air-sea temperature difference is modest, and so high buoyancy flux requires strong winds. These strong winds also drive strong waves. Hence strong buoyancy forcing is accompanied by strong wave forcing. The deep mixed layers shown in Figures 5 and 6 are in the vicinity of the sub-Antarctic front where the sea surface temperature has a strong gradient [*Dong et al.*, 2008]. Winds blowing across the front become relatively dry and create strong air-sea temperature contrasts, so buoyancy fluxes are large even at moderate wind speeds. Cold, dry air outbreaks from land to warm ocean similarly produce strong heat fluxes for moderate winds. Data from the Östergarnsholm site in the Baltic Sea suggest buoyancy forcing dominates there about 20% of the time. Hence we see that wave forcing is important even when buoyancy forcing is present, except at edges of ocean basins or in certain special regions of the ocean where large-scale ocean dynamics produce strong surface temperature gradients.

4. Potential Impacts of Langmuir Turbulence

[28] The regime diagram in Figure 3 shows contours of the joint histogram of the La and h/L_L in the Southern Ocean during winter. The joint histogram suggests wave and buoyancy forcing to be important mechanisms of turbulence production in the mixed layer of the OSBL in this region. But if wave forcing and Langmuir turbulence is so prevalent, and since wind and waves always occur together, perhaps current parameterizations already implicitly account for the effects of wave forcing? This might circumvent the need to account explicitly for wave driven turbulence if wind and waves were in fully-developed equilibrium. Indeed, there is

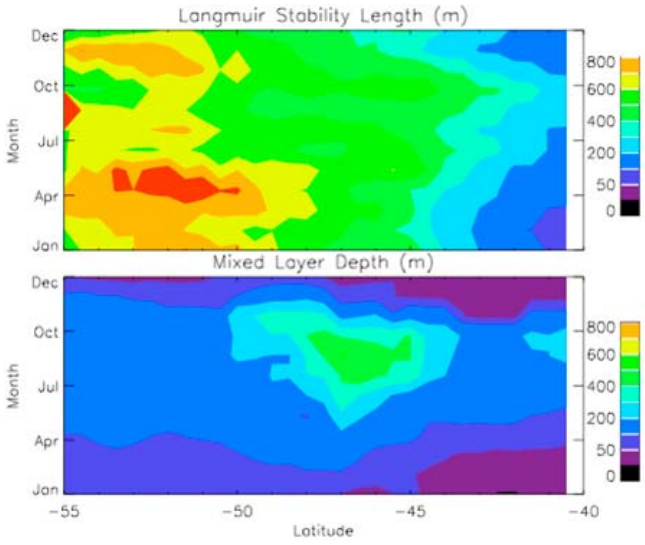

Figure 6. Annual evolution of the roles of convective forcing and wave forcing in the Southern Ocean. Contours show a Hovmoller plot of (top) Langmuir-stability length and (bottom) mixed layer depth and along the line A-B in Figure 5, which cuts across the sub-Antarctic front. When $h > L_L$ convective forcing dominates, whereas when $h < L_L$ wave forcing dominates.

then a relation between the surface wind speed and the wave spectrum, and hence the Stokes drift, and so the wave forcing. But this is an unsatisfactory approach because *Sullivan et al.* [2008] and *Hanley et al.* [2010] show that wind and waves are rarely in equilibrium. This finding is supported here by the large dynamic range of *La*, which would not be seen if the wind and wave forcings were always in a constant ratio. Misaligned waves and winds tend to increase this dynamic range [*Van Roekel et al.*, 2012]. Since wave-driven turbulence mixes and entrains differently compared to wind-driven turbulence, these two processes cannot then be tuned with a single parameter. Langmuir turbulence needs to be parameterized as a mechanism in its own right. So, what are the likely effects of representing wave-forcing and Langmuir turbulence in parameterizations of the OSBL? Firstly, LES suggests that in certain circumstances wave forcing can lead to large changes in the mixing profile through the OSBL and the entrainment flux at the base of the OSBL. In a particular example, with the global mean value of La = 0.4, the entrainment flux at the base of the mixed layer in LES is a factor 3 times higher with wave-forced than for wind-forced turbulence [see *Grant and Belcher*, 2009, Figure 16]. *Smyth et al.* [2002] show how inclusion of Langmuir turbulence improves LES of mixed layer shear in the western tropical Pacific.

[29] Current climate models also ignore other processes that are known to be important in deepening the OSBL. Firstly, *Large and Crawford* [1995] show that inertial oscillations are generated in the OSBL by rapidly-varying winds, which in turn are effective at deepening the OSBL. Measurements by *Ledwell et al.* [2011] show strong inertial oscillations in the Southern Ocean. But this process is not currently represented in climate models because (i) the ocean models are typically forced with daily-mean winds, and (ii) the ocean models are too viscous to allow realistic inertial oscillations. Furthermore, our present understanding of this process is not mature: for example, tentative results from *Grant and Belcher* [2011] suggest that this process may be effective only when fh/u_* is small. Secondly, the interaction of winds with submesoscale eddies and fronts, which are also un-resolved in global ocean models, can generate both mixing and restratification in the OSBL [e.g., *Thomas and Lee*, 2005; *Fox-Kemper et al.*, 2008]. Again our understanding is not mature: there are competing effects, so for example it is not known whether randomly orientated fronts lead to a net deepening or shoaling of the mixed layer [*Thomas and Ferrari*, 2008; *Mahadevan et al.*, 2010]. These processes all deserve further attention.

5. Conclusions

[30] Whilst there are a range of uncertainties in our current understanding of the dynamics of the OSBL, the diagnostic study developed here suggests that turbulent energy available for mixing the OSBL could be grossly underestimated without forcing by surface waves. Wave-forcing and hence Langmuir turbulence could be important over wide areas of the ocean and in all seasons in the Southern Ocean, including during summertime when there are known biases in the OSBL depth in current models. Therefore global climate models need to represent wave forcing of Langmuir turbulence in their parameterizations of the OSBL, which may well require that global climate models also need to compute the surface wave field. There is a pressing need for direct observational evidence to support the results of LES and diagnostic analysis presented here. One way to do this is through continued measurement of turbulence microstructure within the OSBL, for example dissipation rate or vertical velocity variance, and map it on a regime diagram such as in Figure 3.

[31] **Acknowledgments.** We are grateful for useful conversation with Tom Rippeth, Eric D'Asaro, Adrean Webb, Greg Chini, and Keith Julien. SEB and ALMG were supported by NERC under the OSMOSIS project NE/I020083/1. BFK was supported by NASA NNX09AF38G. BFK and LVR were supported by NSF 0934737. PPS and WGL are supported by the National Science Foundation through the National Center for Atmospheric Research. PPS also acknowledges support from the Office of Naval Research. JAP is funded under NERC grant NE/I002103/1.

[32] The Editor thanks two anonymous reviewers for assisting in the evaluation of this paper.

References

Boccaletti, G., R. Ferrari, and B. Fox-Kemper (2007), Mixed layer instabilities and restratification, *J. Phys. Oceanogr.*, *37*, 2228–2250, doi:10.1175/JPO3101.1.

Craik, A. D. D., and S. Leibovich (1976), Rational model for Langmuir circulations, *J. Fluid Mech.*, *73*, 401–426, doi:10.1017/S0022112076001420.

D'Asaro, E., C. Lee, L. Rainville, R. Harcourt, and L. Thomas (2011), Enhanced turbulence and energy dissipation at ocean fronts, *Science*, *332*, 318–322, doi:10.1126/science.1201515.

de Boyer Montégut, C., G. Madec, A. S. Fischer, A. Lazar, and D. Iudicone (2004), Mixed layer depth over the global ocean: An examination of profile data and a profile-based climatology, *J. Geophys. Res.*, *109*, C12003, doi:10.1029/2004JC002378.

Dee, D. P., et al. (2011), The ERA-Interim reanalysis: Configuration and performance of the data assimilation system, *Q. J. R. Meteorol. Soc.*, *137*, 553–597, doi:10.1002/qj.828.

Dong, S., J. Sprintall, S. T. Gille, and L. Talley (2008), Southern Ocean mixed-layer depth from Argo float profiles, *J. Geophys. Res.*, *113*, C06013, doi:10.1029/2006JC004051.

Fox-Kemper, B., R. Ferrari, and R. W. Hallberg (2008), Parameterization of mixed layer eddies. Part I: Theory and diagnosis, *J. Phys. Oceanogr.*, *38*(6), 1145–1165, doi:10.1175/2007JPO3792.1.

Fox-Kemper, B., G. Danabasoglu, R. Ferrari, S. M. Griffies, R. W. Hallberg, M. M. Holland, M. E. Maltrud, S. Peacock, and B. L. Samuels (2011), Parameterization of mixed layer eddies. III: Implementation and impact in global ocean climate simulations, *Ocean Modell.*, *39*, 61–78, doi:10.1016/j.ocemod.2010.09.002.

Grant, A. L. M., and S. E. Belcher (2009), Characteristics of Langmuir turbulence in the ocean mixed layer, *J. Phys. Oceanogr.*, *39*(8), 1871–1887, doi:10.1175/2009JPO4119.1.

Grant, A. L. M., and S. E. Belcher (2011), Wind-driven mixing below the oceanic mixed layer, *J. Phys. Oceanogr.*, *41*(8), 1556–1575, doi:10.1175/JPO-D-10-05020.1.

Hanley, K. E., S. E. Belcher, and P. P. Sullivan (2010), A global climatology of wind wave interaction, *J. Phys. Oceanogr.*, *40*, 1263–1282, doi:10.1175/2010JPO4377.1.

Harcourt, R. R., and E. A. D'Asaro (2008), Large-eddy simulation of Langmuir turbulence in pure wind seas, *J. Phys. Oceanogr.*, *38*(7), 1542–1562, doi:10.1175/2007JPO3842.1.

Hewitt, H. T., D. Copsey, I. D. Culverwell, C. M. Harris, R. S. R. Hill, A. B. Keen, A. J. McLaren, and E. C. Hunke (2010), Design and implementation of the infrastructure of HadGEM3: The next-generation Met Office climate modelling system, *Geosci. Model Dev. Discuss.*, *3*, 1861–1937, doi:10.5194/gmdd-3-1861-2010.

Kenyon, K. E. (1969), Stokes drift for random gravity waves, *J. Geophys. Res.*, *91*, 191–208.

Large, W. G., and G. B. Crawford (1995), Observations and simulations of upper-ocean response to wind events during the Ocean Storms experiment, *J. Phys. Oceanogr.*, *25*, 2831–2852, doi:10.1175/1520-0485(1995)025<2831:OASOUO>2.0.CO;2.

Large, W. R., J. C. McWilliams, and S. C. Doney (1994), Oceanic vertical mixing: A review and a model with a non-local boundary layer parameterization, *Rev. Geophys.*, *32*, 363–403, doi:10.1029/94RG01872.

Ledwell, J. R., L. C. St Laurent, J. B. Girton, and J. M. Toole (2011), Diapycnal mixing in the Antarctic Circumpolar Current, *J. Phys. Oceanogr.*, *41*, 241–246, doi:10.1175/2010JPO4557.1.

Leibovich, A. (1983), The form and dynamics of Langmuir circulations, *Annu. Rev. Fluid Mech.*, *15*, 391–427, doi:10.1146/annurev.fl.15.010183.002135.

Li, M., C. Garrett, and E. Skyllingstad (2005), A regime diagram for classifying turbulent large eddies in the upper ocean, *Deep Sea Res., Part I*, *52*, 259–278, doi:10.1016/j.dsr.2004.09.004.

Mahadevan, A., A. Tandon, and R. Ferrari (2010), Rapid changes in mixed layer stratification driven by submesoscale instabilities and winds, *J. Geophys. Res.*, *115*, C03017, doi:10.1029/2008JC005203.

McWilliams, J. C., P. P. Sullivan, and C. H. Moeng (1997), Langmuir turbulence in the ocean, *J. Fluid Mech.*, *334*, 1–30, doi:10.1017/S0022112096004375.

Moeng, C. H., and P. P. Sullivan (1994), A comparison of shear- and buoyancy-driven planetary boundary layer flows, *J. Atmos. Sci.*, *51*, 999–1022, doi:10.1175/1520-0469(1994)051<0999:ACOSAB>2.0.CO;2.

Monterey, G., and S. Levitus (1997), *Seasonal Variability of Mixed Layer Depth for the World Ocean, NOAA Atlas NESDIS*, vol. 14, 100 pp., NOAA, Silver Spring, Md.

Pierson, W. J., and L. Moskowitz (1964), A proposed spectral form for fully developed wind seas based on the similarity theory of S A Kitaigorodskii, *J. Geophys. Res.*, *69*, 5181–5190, doi:10.1029/JZ069i024p05181.

Polton, J. A., and S. E. Belcher (2007), Langmuir turbulence and deeply penetrating jets in an unstratified mixed layer, *J. Geophys. Res.*, *112*, C09020, doi:10.1029/2007JC004205.

Rutgersson, A., M. Norman, B. Schneider, H. Pettersson, and E. Sahlée (2008), The annual cycle of carbon-dioxide and parameters influencing the air-sea carbon exchange in the Baltic Proper, *J. Mar. Syst.*, *74*, 381–394, doi:10.1016/j.jmarsys.2008.02.005.

Skyllingstad, E. D., and D. W. Denbo (1995), An ocean large-eddy simulation of Langmuir circulations and convection in the surface mixed layer, *J. Geophys. Res.*, *100*(C5), 8501–8522, doi:10.1029/94JC03202.

Smedman, A., U. Högström, H. Bergström, A. Rutgersson, K. Kahma, and H. Pettersson (1999), A case-study of air-sea interaction during swell conditions, *J. Geophys. Res.*, *104*, 25,833–25,851, doi:10.1029/1999JC900213.

Smyth, W. D., E. D. Skyllingstad, G. B. Crawford, and H. Wijesekera (2002), Nonlocal fluxes and Stokes drift effects in the K-profile parameterization, *Ocean Dyn.*, *52*, 104–115, doi:10.1007/s10236-002-0012-9.

Sullivan, P. P., and J. C. McWilliams (2010), Dynamics of winds and currents coupled to surface waves, *Annu. Rev. Fluid Mech.*, *42*, 19–42, doi:10.1146/annurev-fluid-121108-145541.

Sullivan, P. P., J. C. McWilliams, and W. K. Melville (2007), Surface gravity wave effects in the oceanic boundary layer: Large eddy simulation with vortex force and stochastic breakers, *J. Fluid Mech.*, *593*, 405–452, doi:10.1017/S002211200700897X.

Sullivan, P. P., J. B. Edson, T. Hristov, and J. C. McWilliams (2008), Large-eddy simulations and observations of atmospheric marine boundary layers above nonequilibrium surface waves, *J. Atmos. Sci.*, *65*, 1225–1245, doi:10.1175/2007JAS2427.1.

Teixeira, M. A. C., and S. E. Belcher (2002), On the distortion of turbulence by a progressive surface wave, *J. Fluid Mech.*, *458*, 229–267, doi:10.1017/S0022112002007838.

Teixeira, M. A. C., and S. E. Belcher (2010), On the structure of Langmuir turbulence, *Ocean Modell.*, *31*(3–4), 105–119, doi:10.1016/j.ocemod.2009.10.007.

Terray, E. A., et al. (1996), Estimates of kinetic energy dissipation under breaking waves, *J. Phys. Oceanogr.*, *26*, 792–807, doi:10.1175/1520-0485(1996)026<0792:EOKEDU>2.0.CO;2.

Thomas, L. N., and R. Ferrari (2008), Friction, frontogenesis, and the stratification of the surface mixed layer, *J. Phys. Oceanogr.*, *38*, 2501–2518, doi:10.1175/2008JPO3797.1.

Thomas, L. N., and C. M. Lee (2005), Intensification of ocean fronts by down-front winds, *J. Phys. Oceanogr.*, *35*, 1086–1102, doi:10.1175/JPO2737.1.

Thorpe, S. A. (2005), *The Turbulent Ocean*, 121 pp., Cambridge Univ. Press, Cambridge, U. K., doi:10.1017/CBO9780511819933.

Uppala, S. M., et al. (2005), The ERA-40 re-analysis, *Q. J. R. Meteorol. Soc.*, *131*, 2961–3012, doi:10.1256/qj.04.176.

Van Roekel, L. P., B. Fox-Kemper, P. P. Sullivan, P. E. Hamlington, and S. R. Haney (2012), The form and orientation of Langmuir cells for misaligned winds and waves, *J. Geophys. Res.*, *117*, C05001, doi:10.1029/2011JC007516.

Webb, A., and B. Fox-Kemper (2011), Wave spectral moments and Stokes drift estimation, *Ocean Modell.*, *40*(3–4), 273–288, doi:10.1016/j.ocemod.2011.08.007.

Weijer, W., et al. (2012), The Southern Ocean and its climate in CCSM4, *J. Clim.*, *25*, 2652–2675, doi:10.1175/JCLI-D-11-00302.1.